Prediction of Niño 3 Sea Surface Temperatures Using Linear Inverse Modeling

CÉCILE PENLAND AND THERESA MAGORIAN

Cooperative Institute for Research in Environmental Sciences, University of Colorado, Boulder, Colorado

(Manuscript received 14 October 1991, in final form 15 October 1992)

ABSTRACT

Linear inverse modeling is used to predict sea surface temperatures (SSTs) in the Niño 3 region. Predictors in three geographical locations are used: the tropical Pacific Ocean, the tropical Pacific and Indian oceans, and the global tropical oceans. Predictions did not depend crucially on any of these three domains, and evidence was found to support the assumption that linear dynamics dominates most of the record. The prediction model performs better when SST anomalies are rapidly evolving than during warm events when large anomalies persist. The rms prediction error at a lead time of 9 months is about half a degree Celsius.

1. Introduction

A statistical prediction method based on principal oscillation pattern (POP) analysis (Hasselmann 1988; Von Storch et al. 1988) is used to forecast sea surface temperatures (SSTs) in the region of the equatorial Pacific Ocean known as Niño 3. The original POP analysis was concerned with predicting the phase of a particular, subjectively selected complex normal mode, or POP, of the deterministic feedback matrix. Xu and von Storch (1990) have used this version of POP analysis to find a pair of damped oscillatory patterns closely associated with the Southern Oscillation and characterized by a single oscillation period of about three years. It has been shown (Penland 1989) how groups of normal modes can be combined to predict a measured field in a chosen geographical location. In this study, we use that technique to predict sea surface temperatures (SSTs) in the Niño 3 region of the Pacific. Representing several frequencies in the prediction, rather than just one, can be expected to yield better forecasts of what is actually measured, although the simplicity of interpreting a single cyclic phenomenon is sacrificed.

Like canonical correlation analysis (CCA: Barnett et al. 1988; Graham et al. 1987a,b), our technique involves a linear transformation of a predictor field to produce a forecast of a predictand field. Here, the predictand field is the predictor field at some later time. CCA derives a transformation that *maximizes the correlation* between the predictand and the transformed predictor field. In contrast, POP analysis is based on an eigenvalue problem resulting from *minimizing the error* between the predictand and the transformed predictor field. Estimations of the transformation matrices, or Green functions, are obtained directly from the multivariate time series data. Also, the dynamics of the system is assumed to be continuous and linearly Markovian. Our analysis, therefore, is equivalent to linear inverse modeling.

This article is less concerned with statistical prediction in general than it is with the role of empirically derived normal modes in this method of forecasting, with emphasis placed on the collective behavior of the modes. The linear nature of the assumed dynamical model precludes the identification of unstable, growing modes since such modes would grow without bound in a stationary linear system. The physical system at hand is nonlinear and admits instabilities, such as Legeckis waves, which grow by drawing energy from the mean flow until nonlinear wave dynamics become important enough to stabilize the system. How, then, is a forecasting technique based on a linear model justified?

As noted in Blumenthal (1991), the POP analysis fits the data with the best globally linear system having climatology as the attracting fixed point and includes a weighted average of the nonlinear dynamics. The analysis is most useful when the data under scrutiny can be themselves temporally averaged over periods long compared with time scales of the nonlinear effects, so that any nonlinearities can be treated as white noise. The 3-month running means of monthly averaged SSTs considered here satisfy this condition when compared with Legeckis waves, which develop and propagate on time scales of a few weeks (Legeckis 1977; Philander et al. 1985). In contrast, time scales associated with nonlinear propagation of Kelvin and Rossby waves important to the El Niño–Southern Oscillation (ENSO) phenomenon are of the same order as, or longer than, the period over which our data are averaged (Philander 1990), so it is not clear a priori what

Corresponding author address: Dr. Cecile Penland, CIRES, University of Colorado, Campus Box 449, Boulder, CO 80309-0449.

effect these nonlinearities will have on the analysis. Nevertheless, it is shown in this article that the assumption of stable linear dynamics is surprisingly good for making predictions with lead times up to about nine months if the collective behavior of the empirically derived modes is exploited.

The "collective behavior" meant here is the summed effect of the generally non-self-adjoint normal modes. The variance contained in a field of normal modes is not equal to the sum of variances the individual modes would have were each propagating by itself, and the difference is due to the constructive or destructive interference in the modal superposition. Note that empirical orthogonal functions (EOFs), on average, do not interact energetically; the variance of the field is equal to the sum of the variances contained in the individual EOFs. (The pernicious habit of calling EOFs "modes" sometimes leads researchers to confuse the properties of EOFs and normal modes, which are eigenfunctions of a linearized dynamical system.) Both the untruncated set of EOFs and the set of empirically derived normal modes are complete on the measurement space, and a multivariate field or perturbation thereof can be described in terms of either set of functions. "Transient perturbation growth" or "nonmodal growth" (Farrell 1988, 1989, 1990; Blumenthal 1991; Borges and Hartmann 1992) occurs when normal modes contributing to a perturbation interfere in an increasingly constructive manner for a while, thus allowing the amplitude of the perturbation to increase even though individual modes necessary to the growth may in fact be decaying modes. It is easy to see that the phase interference of contributing normal modes is also responsible for the group velocities of "nonmodal" traveling disturbances. One purpose of this article is to investigate whether the variation of Niño 3 SST is dominated by a single empirically derived normal-mode pair, or whether this variation is a "nonmodal" conspiracy of normal modes having several frequencies.

Section 2 of this article describes the data and how they were prepared for application of the prediction technique. The prediction technique itself is described in section 3. Unlike previous expositions (Penland 1989; Penland and Ghil 1991, 1993) the technique is presented here as applied to a set of principal components (PCs) rather than to the multivariate time series in geographical space. The formalism applied in either space, however, is identical to that applied in the other, so this should not be confusing. The results of our analysis are exposed in section 4 and discussed in section 5.

2. The dataset

The analysis was applied to monthly averaged SSTs obtained from the comprehensive ocean–atmosphere dataset (Slutz et al. 1985). The data were available on a $2° \times 2°$ grid, which we consolidated into a $4° \times 10°$ grid, requiring four of the ten original grid squares to have data at any particular month to be considered an observation. The grand mean and the phase-averaged annual cycle were removed, and a 3-month running mean time series was obtained from the monthly averaged SST data, which were otherwise unfiltered. Our predictands are the average SST in a region containing Niño 3 (8°N–8°S; 150°W–90°W), hereafter designated as such. We considered the time period January 1950–December 1984 for the training period and verified on the time after that (January 1985–November 1990). This verification period is somewhat short. Given the periodicities required to adequately describe the data; however, a shorter training period could not be tolerated and the six years of verification do include an entire warm event and an entire cold event. In choosing predictors for SSTs in Niño 3, SSTs in three tropical (32°N–32°S) ocean domains were considered: the Pacific (Pac: 100°E–70°W), the Indian–Pacific (PacIn: 30°E–70°W), and the global tropical oceans (Glob).

Empirical orthogonal functions (EOFs) were calculated for each domain. Only the training period was used to calculate the EOFs, which were used as an orthonormal basis onto which to project the entire multivariate time series. The leading EOF in any of the domains is indistinguishable from the leading EOF in the others and is dominated by an equatorial Pacific pattern (not shown). The leading ten principal components (PCs) explain 60%, 57%, and 51% of the training period variance in the Pac, PacIn, and Glob domains, respectively; however, this explained variance is not uniform geographically. Each set of ten EOFs explains 82% of the variance in Niño 3 (total variance $= 0.5°C^2$), and little error is made by considering only their contribution to the SSTs in the region; projecting the data onto the leading ten PCs appears to optimize the signal-to-noise ratio. The time series constructed by combining the ten leading PCs from the PacIn domain and averaging over Niño 3 correlates very highly (98%) with the SST anomaly time series there, insignificantly better than do time series constructed with leading PCs from either Pac or Glob.

3. Prediction technique

Crucial to our predictions is the assumption that the SST anomaly field evolves linearly. This allows us to perform the analysis entirely in EOF space and then transform to geographical space for interpretation. If the SST anomaly field propagates linearly, then so do its PCs. For M retained EOFs, the αth principal component $c_\alpha(t)$ is assumed to evolve as

$$\frac{dc_\alpha}{dt} - \sum_{\kappa=1}^{M} \mathbf{B}_{\alpha\kappa} c_\kappa = \epsilon_\alpha + \xi_\alpha, \qquad (1)$$

where $\mathbf{B}$ is a deterministic, constant $M \times M$ matrix, and ϵ_α is the error in the αth PC tendency due to linear

interactions between retained and neglected PCs. We ignore ϵ_α completely. The quantity ξ_α represents not only subgrid and subscale processes but also nonlinear effects; it is assumed that this can be treated as a Gaussian white noise forcing of the αth PC.

A prediction of the PC field at time $t + \tau$ is made from the PC field at time t, $\mathbf{c}(t)$, via a *Green function* $\mathbf{G}(\tau)$. Given $\mathbf{c}(t)$ and Eq. (1) (with ϵ_α neglected), prediction of the most probable $\mathbf{c}(t + \tau)$ at later time $t + \tau$ is $\mathbf{G}(\tau)\mathbf{c}(t)$. We calculate the Green function by choosing some lag τ_0 and forming the matrix $\mathbf{G}(\tau_0)$ whose elements are

$$\mathbf{G}_{\alpha\beta}(\tau_0) \equiv \langle c_\alpha(t + \tau_0)c_\beta(t)\rangle/\lambda_\beta, \qquad (2)$$

where angle brackets indicate expectation values. The βth EOF eigenvalue λ_β is $\langle c_\beta^2(t)\rangle$. The eigenvalues $\{g_n(\tau_0)\}$ of $\mathbf{G}(\tau_0)$, along with the corresponding eigenvectors $\{\mathbf{u}_n\}$ and adjoint eigenvectors $\{\mathbf{v}_n\}$, are then combined to obtain the Green function at *any* lag τ (Penland 1989):

$$\mathbf{G}(\tau) = \sum_{n=1}^{M} \mathbf{u}_n[g_n(\tau_0)]^{\tau/\tau_0}\mathbf{v}_n^T. \qquad (3)$$

The eigenvalues $\{g_n(\tau_0)\}$ of $\mathbf{G}(\tau_0)$ are either complex, giving both a decay time and a period of oscillation to each complex mode $\mathbf{u}_n$, or real, in which case $\mathbf{u}_n$ is simply an exponentially decaying structure maintained by unresolved processes. Complex eigenvalues and their corresponding eigenmodes occur in complex conjugate pairs. For a truly linear Markov process, $\mathbf{G}(\tau)$ is independent of τ_0. For a real system where nonlinearities affect dynamics, the Green function must be calculated at a variety of lags τ_0 to estimate the error inherent in the assumption of linear dynamics. In the following, the Green function at lag τ calculated with parameters obtained with specified lag τ_0 [Eq. (3)] is denoted $\mathbf{G}(\tau; \tau_0)$.

Given the PC field $\mathbf{c}(t)$ at time t and Green functions obtained with lag τ_0, the most probable value $\hat{x}_i(t + \tau)$ of the SST anomaly field $x_i(t + \tau)$ at later time $t + \tau$ and geographical location i is

$$\hat{x}_i(t + \tau) = \sum_{\alpha,\beta=1}^{M} \varphi_{i\alpha}\mathbf{G}_{\alpha\beta}(\tau; \tau_0)c_\beta(t), \qquad (4)$$

where $\varphi_{i\alpha}$ is the value of the αth EOF at location i. The prediction of the average SST anomaly field in Niño 3 is obtained by taking the average of $\hat{x}_i(t + \tau)$ for all locations i within the region.

Although we have presented the procedure in EOF space, the linear dynamical model allows an equivalent formalism in geographical space. In geographical space, the vector of PCs $\mathbf{c}(t)$ is replaced by the SST anomaly field $\mathbf{x}(t)$, where $x_i(t)$ is the SST anomaly at location i and time t. Just as the PC field $\mathbf{c}(t)$ is related to the anomaly field $\mathbf{x}(t)$ through a simple linear transformation involving the EOFs, each eigenvector $\mathbf{u}_n$ calculated in EOF space is associated with a geographical pattern $\tilde{\mathbf{u}}_n$, evolving with the same time scales as in EOF space, and obtained in the same way that $\mathbf{x}(t)$ is obtained from $\mathbf{c}(t)$. This pattern $\tilde{\mathbf{u}}_n$ is an eigenvector of the Green function in geographical space.

4. Results

a. Domain dependence and phase interference

As discussed in section 3, the average SST anomaly in the Niño 3 region is not strongly affected by first projecting the SST anomalies onto the leading ten PCs calculated in any of the three oceanic domains. Although EOFs are notoriously domain dependent, the tropical Pacific is active enough that the leading EOFs, particularly the first three, calculated in any of the three domains are dominated by high loadings there. Using the first ten PCs of SSTs in each region as predictors, the eigenvalues and eigenfunctions of $\mathbf{G}(\tau_0; \tau_0)$ were calculated for $\tau_0 = 7$ months and combined as in Eqs. (3)–(4) to predict the SST anomalies in Niño 3. This value of τ_0 is representative of the *e*-folding times of the various eigenmodes (Table 1) and was chosen to minimize the error in the empirically obtained eigenvalues due to the finite length of the time series (Penland and Ghil 1989).

Figure 1 shows the root-mean-square (rms) error in prediction as a function of lead time τ for the various regions, as well as the rms errors in prediction by persistence, and in prediction by univariate autoregressive (AR) processes (Chu and Katz 1985). Predictions are verified against data that have *not* been subjected to the EOF-filtering process; the error curves therefore include the prediction error caused by using only ten PCs. Each set of multivariate predictions based on PCs calculated in a particular domain performs about as

TABLE 1. Time scales associated with empirically derived normal modes.

Mode number	Decay time (months)	Period (months)
	Pacific	
1/2	15	94
3/4	12	313
5	10	N/A
6/7	9	31
8	4	N/A
9	4	N/A
10	1	N/A
	Pacific–Indian	
1/2	18	284
3/4	13	139
5/6	9	65
7/8	8	29
9/10	5	39

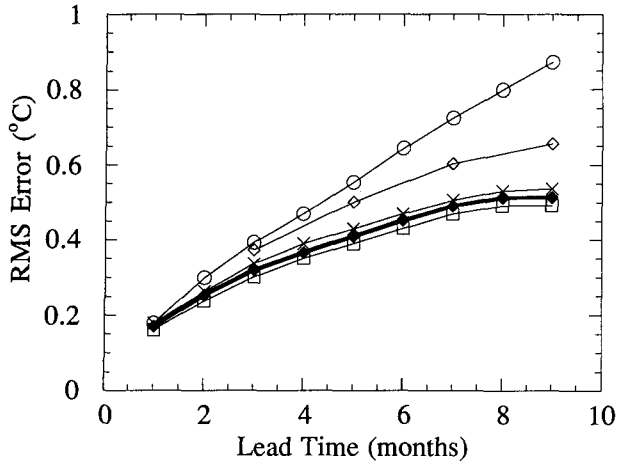

FIG. 1. Root-mean-square prediction error as a function of lead time in Niño 3 using PCs calculated in Pac (squares), Pacin (filled diamonds), and Global (× signs) tropical oceans. For comparison is the rms error incurred by prediction by persistence (circles) and by a univariate autoregression (AR) process (open diamonds).

well as the other two, with the rms prediction error varying among them by only a few hundredths of a degree. These multivariate linear predictions do, however, predict Niño 3 SST anomalies consistently better than persistence or the univariate AR process.

The apparent invariance of the predictions with these geographical domains raises several questions. In particular, is the prediction due mainly to a dominant domain-invariant pair of modes in the summation (3)? Are *most* of the modes invariant with the domain in which they are calculated or does each set of modes have little in common with the other two sets, yet act in concert to describe the same field as the others? To answer these questions, we consider the individual modes obtained in the Pac and PacIn regions. The time scales associated with these modes are given in Table 1. The modes were transformed into geographical space and the magnitude of the complex pattern correlation between the two sets of modes was calculated for that geographical region where they both had loadings, that is, the tropical Pacific. It was found that many of the modes of one region are highly correlated with modes of the other, but this correlation is not one to one. For example, the 6/7 mode pair of the Pacific region is correlated at 82% with the 5/6 mode pair of the PacIn region, and with the PacIn 7/8 mode pair at 95%, even though the Pac 6/7 mode pair and the PacIn 7/8 mode pair are the only ones in the two sets that unambiguously correspond (see Fig. 5). Of course, several modes within any set are themselves highly correlated and probably represent related physical processes.

The importance of this phase interference is emphasized by considering the contributions to the Niño 3 SST field by the individual modes. We decomposed the Green function $\mathbf{G}(\tau; \tau_0)$ into K matrices $\mathbf{G}_k(\tau; \tau_0)$, where $\mathbf{G}_k(\tau; \tau_0)$ is the contribution to the summation (3) from the kth mode structure, which will be either one real mode or one complex conjugate pair. Here K is the number of complex conjugate pairs plus the number of exponentially decaying structures. That is, $K = 7$ for the Pac region and $K = 5$ for PacIn. The matrix $\mathbf{G}_k(\tau = 0; \tau_0)$ when applied to the SST field unambiguously projects out the contribution to the field by the kth mode structure at $\tau = 0$, independent of normalization. The partial Green function $\mathbf{G}_k(\tau; \tau_0)$ applied to the SST field allows the evolution of that kth mode structure to be predicted. The rms error in describing the entire Niño 3 SST anomaly field by each of the individual normal-mode structures as predicted by the linear model is shown in Fig. 2. None of the individual error curves goes smoothly to zero at zero lead time since none of the mode structures can de-

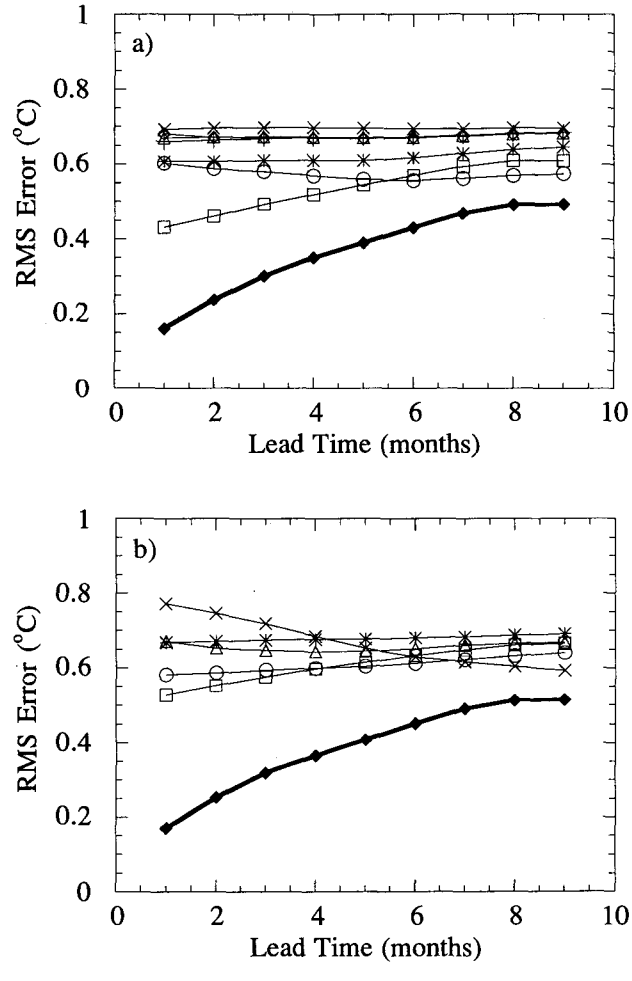

FIG. 2. Root-mean-square prediction error as a function of lead time in using all ten leading PCs (solid diamonds) in (a) Pac and (b) PacIn regions, compared with prediction using individual real modes or complex mode pairs. (a) Pac region. Circles: modes 1/2. Asterisks: modes 3/4. × signs: mode 5. Squares: modes 6/7. Triangles: mode 8. Plus signs: mode 9. Open diamonds: mode 10. (b) PacIn region. Circles: modes 1/2. Asterisks: modes 3/4. × signs: modes 5/6. Squares: modes 7/8. Triangles: modes 9/10.

scribe the SST field by itself and, of course, predictions made this way are much worse than those made using the combined Green function $\mathbf{G}(\tau; \tau_0)$. It is interesting, however, to remark that none of the error curves using just one mode or mode pair has the same monotonic curvature as that obtained with $\mathbf{G}(\tau; \tau_0)$, and that none stands out as making significantly better predictions than the others. Finally, we note that the individual error curves in the Pac and PacIn regions do not look alike, although the error curves using $\mathbf{G}(\tau; \tau_0)$ calculated in the respective regions do.

Another less quantitative measure of the importance of wave variance contained in the correlations between modes is given by the relative error curves calculated for the PacIn region and shown in Fig. 3. Here, the rms error in predicting the amplitude of each mode structure is shown relative to the standard deviation of that mode. Also shown is the relative error in predicting the Niño 3 SSTs using the combined Green function. The error curves for the individual modes vary as expected between 0 and $2^{1/2}$ and approach unity much more quickly than the error curve obtained using the combined Green function.

We must conclude that linear inverse-modeling predictions of SSTs in Niño 3 using the leading ten PCs as predictors does not depend on whether the PCs and empirically derived modes were calculated in the Pacific, the Pacific–Indian, or the global tropical ocean domain. This independence of domain is not due to a single dominant, domain-independent mode, although the modes calculated in different regions are highly correlated and some are very similar. Rather, the modes calculated in any of the three domains have large loadings in the Pacific and act together to describe the SST anomaly field.

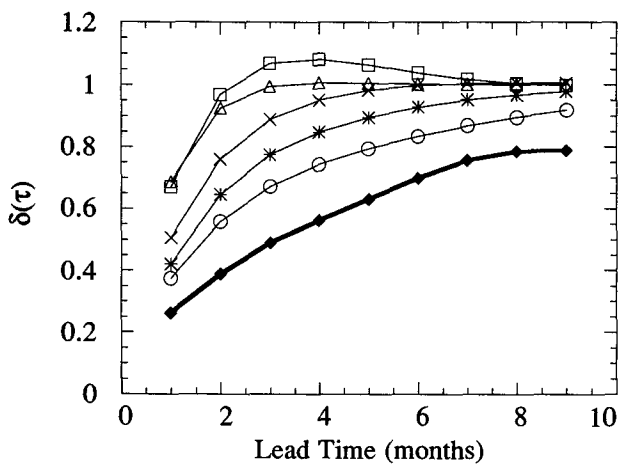

FIG. 3. Ratio of rms error in predicting individual mode amplitudes to standard deviation of corresponding modes. Symbols as in Fig. 2b. Also shown (filled diamonds) is ratio of rms error in predicting SST field using all ten PCs to the standard deviation of SSTs in Niño 3.

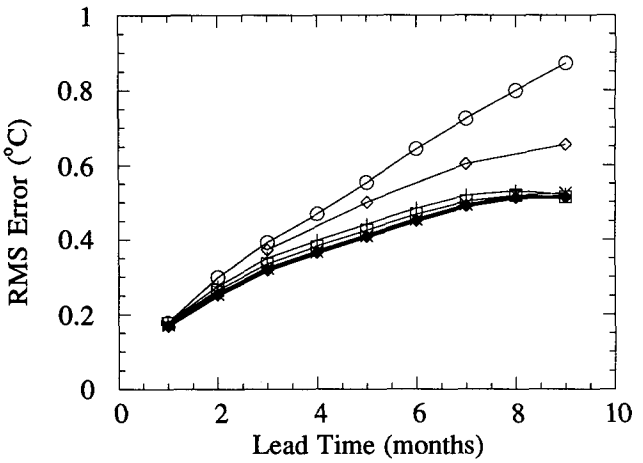

FIG. 4. Root-mean-square prediction error as a function of lead time. Circles: Persistence. Open diamonds: univariate AR process. × signs: τ_0 = 5 months. Diamonds: τ_0 = 7 months. Squares: τ_0 = 9 months. Plus signs: τ_0 = 11 months.

b. *The assumption of linear dynamics*

The Green function for a linear dynamical system is independent of τ_0, and the assumption of linearity can be tested by comparing the results obtained with varying τ_0. Using the first ten PCs of SSTs in the PacIn region as predictors, the eigenvalues and eigenfunctions of $\mathbf{G}(\tau_0; \tau_0)$ were calculated for τ_0 = 5, 7, 9, and 11 months and combined as in Eqs. (3)–(4) to predict the SST anomalies. The root-mean-square error in prediction is shown as a function of lead time τ for the various τ_0's, as is the mean square error for prediction by persistence and by a univariate AR process (Fig. 4). For lead times less than 9 months, prediction errors using τ_0 = 5, 7, and 9 months are strikingly similar. This similarity is due to the approximate independence of τ_0 by the eigenvectors and their adjoints, giving credence to the assumption of linear Markovianity within that time frame.

c. *Behavior of a single mode*

Of particular interest is an eigenvector with a decay time of 8–10 months and period of 27–32 months (see also von Storch et al. 1990) found in all of the oceanic basins used in this study. The complex mode 7 found in the PacIn region is examined here. This mode, obtained with τ_0 = 7 months, is dominated by the two leading EOFs (not shown) and exhibits the familiar ENSO pattern (Fig. 5). Looking at the real part of its adjoint (Fig. 6a), we find that a sensitive region is located in the southern Indian Ocean (obviously absent in the Pac case) and could be as important in exciting the 30-month mode as the equatorial Pacific if there were an SST field in the Indian Ocean strong enough to rival the projection onto the adjoint in the Pacific. The imaginary part of the adjoint (Fig. 6b) reveals that

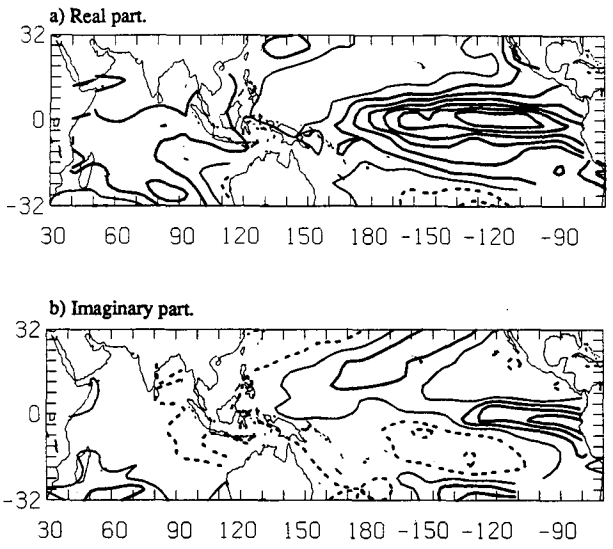

FIG. 5. Eigenvector of $\mathbf{G}$ (τ, τ_0 = 7 months) having decay time of 8 months and an oscillation period of 29 months. Contour interval = 0.025. Solid line: positive loadings. Dashed line: negative loadings. (a) Real part. (b) Imaginary part.

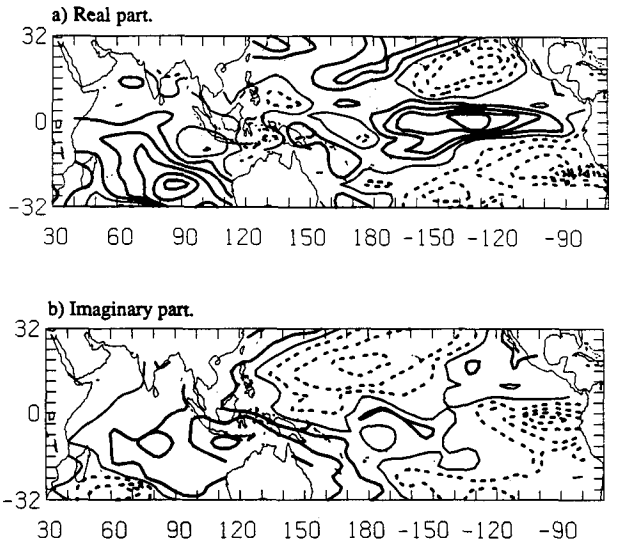

FIG. 6. Adjoint of eigenvector shown in Fig. 6. Contour interval = 0.050. (a) Real part. (b) Imaginary part.

another phase of the 30-month mode is sensitive mainly to Pacific regions.

The amplitude time series of this mode is very noisy and periodic behavior is not immediately obvious. In fact, the short e-folding time compared with the period indicates that either a great deal of noise prohibits prediction of this mode on time scales longer than about 8 months or nonlinearities are important on those time scales. The apparent independence of the results on τ_0 leads us to believe that noise is the culprit, and so we filter the time series coefficients of the complex mode in order to see their behavior. We have chosen an objective method of filtering (Penland et al. 1991, hereafter PGW91; Vautard and Ghil 1989, hereafter VG89; see also Keppenne and Ghil 1991; Weare and Nasstrom 1982) to avoid imposing our prejudices of what the time scales should be. Details of the filtering process are given in PGW91.

Singular spectrum analysis (SSA) was applied separately to the real and imaginary amplitude time series of the complex mode 7 using an embedding dimension of 120. The singular spectra of the two amplitude time series are shown in Fig. 7. The confidence intervals (not shown) of SSA eigenvalues (Fraedrich 1986; VG89) show that a significant break in the singular spectrum of the real part occurs at an SSA index of 17, while 16 significant degrees of freedom were found in the imaginary part. Accordingly, the temporal EOFs and their corresponding temporal PCs were calculated and the significant components recombined to form filtered versions of the real and imaginary amplitude time series of the complex mode 7 (PGW91). The adaptive filtering increased the e-folding time of this mode to about 12 months, an increase of 50%. Behavior of this mode during two typical ENSO events is shown by the familiar Lissajous figures (e.g., Halliday and Resnick 1960; Xu and von Storch 1990) in Fig. 8. Both the period and the phasing of the amplitudes are consistent with the canonical picture of ENSO evolution (Rasmussen and Carpenter 1982).

The pattern correlation between this mode calculated with τ_0 = 7 months and the corresponding mode obtained with τ_0 = 5, 9, and 11 months are 98%, 99%, and 97%, respectively, while the pattern correlation between its adjoint eigenvector obtained with τ_0 = 7 months and the adjoint obtained with τ_0 = 5, 9, and 11 months are 99%, 95%, and 83%, respectively. In fact, *every* mode calculated with τ_0 = 7 months is correlated with a mode calculated with τ_0 = 5 months at

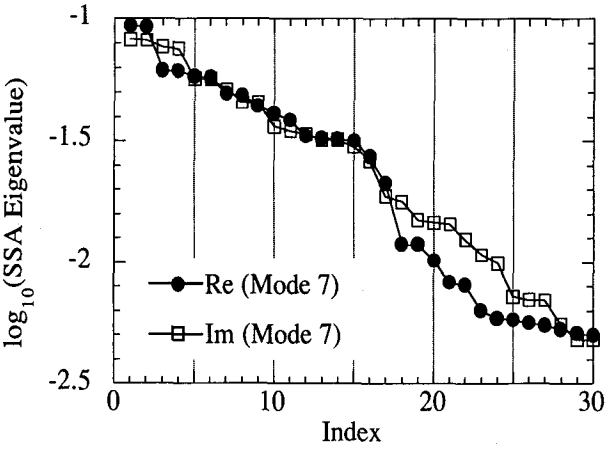

FIG. 7. Singular spectra of empirically derived normal mode time series coefficients. Filled circles: real part. Open squares: imaginary part.

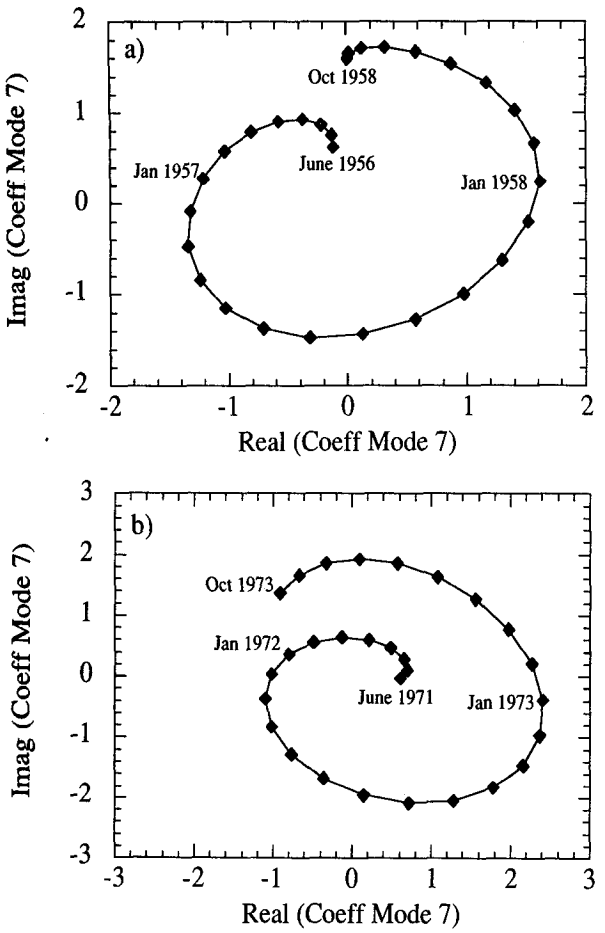

FIG. 8. Lissajous figures formed by plotting the imaginary part of the normal-mode time series coefficient vs the real part. (a) Temporal behavior of mode 7 during 1957/58 ENSO event. (b) Temporal behavior of mode 7 during 1972/73 ENSO event.

a minimum of 76%, and eight of the ten are correlated at a minimum of 93%. The correlations between modes calculated with $\tau_0 = 7$ months and those calculated with $\tau_0 = 9$ months are also highly correlated, with the minimum correlation being 83% and eight out of ten correlating at a minimum of 94%.

d. A closer look at the predictions

Returning our attention to the Niño 3 region, we compare predictions at lead times of 3, 5, 7, and 9 months with verifications of Niño 3 SST anomalies in Fig. 9. Predictions were made with Green functions calculated with $\tau_0 = 7$ months and a training period between January 1950 and December 1984. Also shown is the prediction at a lead time of 7 months made using a univariate AR process (dashed line). The analysis does not like to persist large anomalies and once the anomalies are large enough, it will try to drag them down, as shown by the fact that the only truly terrible predictions occurred during the warm event of 1987. We find that the prediction method performed quite well for periods of rising SST anomalies, with particularly striking agreement between prediction and verification during 1989.

Anomaly correlations between predictions and verifications are misleadingly high (about 0.7 at 9 months; not shown) and manifest the danger of using pattern correlations as a method of verification, particularly when only short verification times are available. The correlations calculated here are not as stable with respect to changes in the verification period as the rms errors; correlations between predictions and verifications depend on *three* quantities involving the length of the verification time series, while the rms error depends on only *one*. More importantly, as lead time increases, the eigenvalues $\{g_n(\tau_0)\}$ require the predicted amplitude of each mode to decay (although the phase of its oscillation may cause a local increase), and correlations cannot detect a consistent over- or underestimation of the *size* of the SST anomaly if the trend of the prediction *at given lead time* follows the trend of the verification. It is for this reason that we have

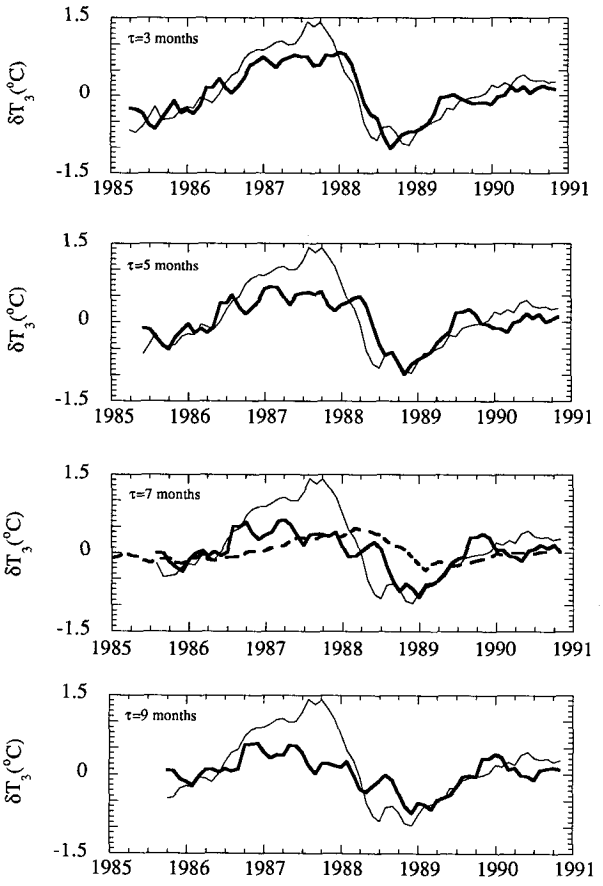

FIG. 9. Comparison of prediction (heavy line: $\tau_0 = 7$ months) and verification (light line) for $\tau = 3$, 5, 7, and 9 months. Also shown is the prediction by a univariate AR process at a lead time of 7 months (dashed line).

chosen to evaluate the model in terms of absolute rms error rather than anomaly correlations.

Linear dynamics driven by Gaussian white noise implies a Gaussian distribution of SST anomalies, and we can use the functional form of the distribution (Wilks 1962; Penland 1989) to calculate confidence intervals for the prediction of the anomaly at any location, or any linear combination of anomaly values at various locations, such as the average SST in Niño 3. Figure 10 shows the prediction (light solid line) of the Niño 3 anomaly based on the PC field of (a) October 1985, (b) January 1987, and (c) August 1988, along with the subsequent verification (heavy solid line). The dashed lines delimit the 95% confidence interval. Although the confidence intervals are large, it is heartening to see that the verification time series is well within the limits during the 1986 period of rising SST anomalies (Fig. 10a). This good case must, however, be contrasted with a bad case, where the model refused to persist a large anomaly that was, indeed, getting larger (Fig. 10b). The excellent agreement between prediction and verification in the one case and the worse performance in the other illustrate how the model failed to predict the duration of a warm event, although the onset was well described. The duration of the 1988/89 cold event, however, was described very well (Fig. 10c), with the fall–winter upturn in SST anomalies being accurately predicted as early as May 1988.

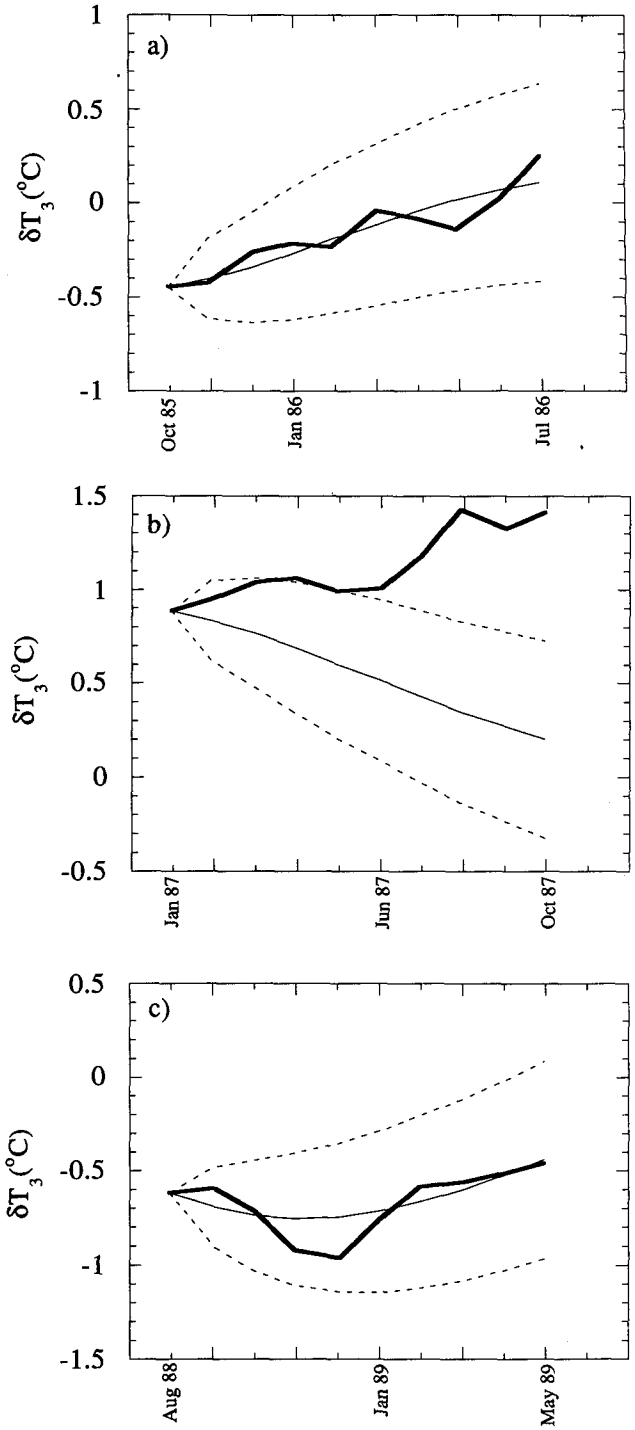

FIG. 10. Prediction of Niño 3 SST, based on PC field of (a) October 1985, (b) January 1987, and (c) August 1988. Dashed lines show 95% confidence interval; the verification is the bold line.

5. Discussion

Prediction of SST anomalies in Niño 3 using ten PCs as predictors is useful up to a lead time of about nine months. There is a trade-off in the number of PCs chosen: 10 PCs try to predict the field with a maximum of five periodicities, but more PCs introduce more noise than signal into the Niño 3 region and make the predictions somewhat less reliable. In fact, we have performed the analysis using 20 PCs and, although more modes are introduced, the difference in rms error in predicting Niño 3 SSTs between the analyses using 10 and 20 PCs is less than 0.04°C at any lag less than nine months (after which the predictions are unreliable anyway), and is usually less than 0.02°C. This is much smaller than any sampling error. In any case, predictions using 10 PCs were verified against SST anomalies in Niño 3, which include *all* the PCs, so that the error curves in Figs. 1, 2, and 4 include the error incurred by retaining only 10 PCs. The fact that the appropriate error curves tend very closely to zero at zero lag indicates that SSTs in Niño 3 are well described with only 10 PCs.

The rms error of prediction does not strongly depend on whether the EOFs, eigenmodes and their adjoints were calculated in the Pacific, Pacific–Indian, or global tropical oceans. The empirically derived eigenmodes are dominated by the Pacific because the retained EOFs were generally dominated by the Pacific. Although many of the eigenmodes calculated in different domains are highly correlated, however, only one pair appears to be identical in the region where all sets have

loadings. The adjoints of modes 6/7 (Pacific) and 7/8 (PacIn), while not identical, are highly correlated (81%) in their common region. An eigenmode or adjoint calculated in, say, the Pacific region is usually highly correlated with more than one mode pair calculated in the Pacific–Indian or global tropical domain. The apparent independence of the prediction on these domains is not due to a single domain-independent mode, but rather to the combined effects of all the modes in a set. That no single mode dominates the SST field is emphasized by the relatively tight bundle of error curves shown in Fig. 2.

Most of the empirically derived normal modes had *e*-folding times that were much smaller than their periods. This does not invalidate the analysis but rather is indicative of the dual nature of an empirically determined *e*-folding time, which can describe either a physical decay rate due to linear, deterministic processes (this is the usual interpretation) or the time during which predictions using the empirically obtained parameters can be trusted (the *linear predictability time*; Penland and Ghil 1991). A perfectly linear process with a lot of noise in it will not be predictable for very long. Nor will a linear process where some important parameters have been omitted, or a nonlinear system where the time scales of nonlinearities are comparable to those of interest. In this study, the average *e*-folding time for the ten modes in either the Pacific or Pacific–Indian region is approximately 9 months, which is about how long our predictions are useful (Figs. 1, 2, and 4). We note, however, that some modes calculated using only Pacific SSTs have *e*-folding times of only 1–4 months, uncomfortably close to or below the lower bound imposed by the 3-month running mean.

Inclusion of Indian Ocean SSTs was necessary to obtain periodicities for most of the empirically derived normal modes. The exception was a mode whose pattern (Fig. 5) and periodicity (29–30 months) strongly suggested a connection with ENSO behavior, but whose *e*-folding time was only about 8–9 months. Adaptive filtering (PGW91) of this mode eliminated much of the noise, and both the period and phasing of the filtered time series were shown to be consistent with canonical ENSO behavior (Rasmussen and Carpenter 1982) during two typical ENSO events (Fig. 8). This reproduction of well-known phenomena verifies the ability of the method to identify physically relevant processes; however, our results do not indicate that a single ENSO mode pair with a single frequency can explain most of the dynamical behavior of the SSTs during an ENSO event.

Agreement of predictions made using Pacific and Pacific–Indian PCs as predictors does not contradict the statement that a sensitive region in exciting an ENSO-like mode lies in the southern Indian Ocean. Excitation of a mode by activity in a localized region requires not only a large loading of the adjoint in that region but also a substantial field to project onto it, and SST variations are considerably weaker in the Indian Ocean than in the Pacific.

Although rms error in predicting SST in Niño 3 using this inverse-modeling technique is better than prediction by either persistence or by a univariate, first-order AR process, the prediction method seems to break down when large warm anomalies persist. As lead time increases, the real part of the mode eigenvalues requires the amplitude of the prediction to decrease, usually causing an underestimation of a large anomaly at long lead times. It is expected, therefore, that the method would describe well the transitions between warm and cold events while inaccurately predicting their duration (Figs. 9–10). The training period necessary to obtain accurate Green functions required a large fraction of the available data, but the verification period was longer than most of the time scales of interest and did contain an entire warm event and an entire cold event. Application of the prediction method to Monterey ship observations during the recent 1991/92 warm event produced prediction–verification plots similar to Fig. 10b, corroborating the conclusion that the method does indeed, as a general rule, break down during warm events if only tropical Pacific–Indian SSTs are used as predictors. On the other hand, the prediction that the 1988/89 cold event would turn around in the late fall–early winter of 1988 was beautifully verified by observation (Fig. 10c). To further illustrate this point, the rms prediction error at a lead time of nine months averaged over the entire verification period was about half a degree Celsius, compared with the rms signal of 0.7°C. The rms error of a 9-month prediction averaged over the verification period but omitting 1987, during which most of the warm event errors occurred, was only a quarter of a degree Celsius (0.25°C).

The dependence of the calculated Green functions on τ_0 was remarkably weak for τ_0 between 5 and 9 months, implying that the first ten PCs of Pacific–Indian SSTs can be assumed to behave as a multivariate linear Markov process on these time scales. This apparent linear behavior is consistent with the work of Barnett et al. (1991) and Lau et al. (1992), which suggest that linear advective processes dominate the equatorial ocean surface heat budget in ocean–atmosphere coupled models. The failure of our empirical model to accurately predict the duration of warm events, however, indicates that linear advection of SSTs is not sufficient to account for their dynamical behavior during a warm event.

SST anomalies in the Niño 3 region are larger than one standard deviation only 14% of the training period, so that the statistically based predictions are dominated by smaller anomalies. This distribution of anomalies itself indicates that our dynamical model, which predicts Gaussian statistics, has limited validity. Repetition of the analysis in the PacIn region, omitting months with Niño 3 anomalies larger than a standard deviation,

resulted in predictions of Niño 3 anomalies with rms errors within two or three hundredths of a degree of the original analysis. Again, these predictions were only weakly dependent on τ_0. Comparison of case studies during the verification period indicate that the broad conclusions are correct: the analysis without the large anomalies could not predict the duration of warm events and performed well during the transition periods (Figs. 10a and 10b were reproduced almost exactly). Somewhat surprisingly, predictions of cold events were degraded with this last analysis, although the verifications were still within the error bars. This indicates that at least some processes operating in cold periods are opposite phases of physical mechanisms operating during warm events. Identifying this symmetric behavior is a topic of current research.

Acknowledgments. The authors are pleased to acknowledge useful conversations with Tim Barnett, Maurice Blackmon, and Prashant Sardeshmukh, and that the questions of a referee resulted in an improved manuscript. We also gratefully acknowledge support by NOAA Grant No. NA16RC0115-01.

REFERENCES

Barnett, T., N. Graham, M. Cane, S. Zebiak, S. Dolan, J. O'Brien, and D. Legler, 1988: On the prediction of the El Niño of 1986–1987. *Nature,* **241,** 192–196.

——, M. Latif, E. Kirk, and E. Roeckner, 1991: On ENSO Physics. *J. Climate,* **4,** 487–515.

Blumenthal, M. B., 1991: Predictability of a coupled ocean–atmosphere model. *J. Climate,* **4,** 766–784.

Borges, M., and D. Hartmann, 1992: Barotropic instability and optimal perturbations of observed nonzonal flows. *J. Atmos. Sci.,* **49,** 335–354.

Chu, P.-S., and R. Katz, 1985: Modeling and forecasting the Southern Oscillation: A time-domain approach. *Mon. Wea. Rev.,* **113,** 1876–1888.

Farrell, B., 1988: Optimal excitation of neutral Rossby waves. *J. Atmos. Sci.,* **45,** 163–172.

——, 1989: Optimal excitation of baroclinic waves. *J. Atmos. Sci.,* **46,** 1193–1206.

——, 1990: Small error dynamics and the predictability of atmospheric flows. *J. Atmos. Sci.,* **47,** 2409–2416.

Fraedrich, K., 1986: Estimating the dimensions of weather and climate attractors. *J. Atmos. Sci.,* **43,** 419–432.

Graham, N. E., J. Michaelsen, and T. P. Barnett, 1987a: An investigation of the El Niño–Southern Oscillation cycle with statistical models. 1. Predictor field characteristics. *J. Geophys. Res.,* **92,** 14 251–14 270.

——, ——, and ——, 1987b: An investigation of the El Niño–Southern Oscillation cycle with statistical models. 2. Model results. *J. Geophys. Res.,* **92,** 14 271–14 289.

Halliday, D., and R. Resnick, 1960: Physics, Parts I and II. John Wiley & Sons, 1214 pp. [See problem 35 of chapter 15.]

Hasselmann, K., 1988: PIPs and POPs—A general formalism for the reduction of dynamical systems in terms of principal interaction patterns and principal oscillation patterns. *J. Geophys. Res.,* **93,** 11 015–11 020.

Keppenne, C., and M. Ghil, 1991: Adaptive spectral analysis and prediction of the Southern Oscillation index. *Proc. 15th Annual Climate Dynamics Workshop,* Asheville, Dept. of Commerce Climate Analysis Center, 30–35 pp.

Lau, N.-C., G. Philander, and M. J. Nath, 1992: Simulation of ENSO-like phenomena with a low-resolution coupled GCM of the global ocean and atmosphere. *J. Climate,* **5,** 284–307.

Legeckis, R., 1977: Long waves in the eastern equatorial Pacific Ocean: A view from a geostationary satellite. *Science,* **197,** 1179–1181.

Penland, C., 1989: Random forcing and forecasting using principal oscillation pattern analysis. *Mon. Wea. Rev.,* **117,** 2165–2185.

——, and M. Ghil, 1989: Use of principal oscillation patterns in forecasting. *Proc. 11th Conf. Probability and Statistics in the Atmospheric Sciences,* Monterey, California, Amer. Meteor. Soc., 16–19.

——, and ——, 1991: Deterministic teleconnections and "random" forcing by transient eedies. *Proc. Eighth Conf. Atmospheric and Oceanic Waves and Stability,* Denver, Amer. Meteor. Soc., 126–129.

——, and ——, 1993: Forecasting Northern Hemisphere 700-mb geopotential height anomalies using empirical normal modes. *Mon. Wea. Rev.,* **121,** in press.

——, ——, and K. Weickmann, 1991: Adaptive filtering and Maximum Entropy Spectra with application to changes in atmospheric angular momentum. *J. Geophys. Res.,* **96,** 22 659–22 671.

Philander, G., 1990: *El Niño, La Niña, and the Southern Oscillation.* Academic Press, Inc., 293 pp.

——, D. Halpern, D. Hansen, R. Legeckis, L. Miller, C. Paul, R. Watts, R. Weisberg, and M. Wimbush, 1985: Long waves in the equatorial Pacific Ocean. *Eos,* **66,** 154–155.

Rasmussen, E., and T. Carpenter, 1982: Variations in tropical sea surface temperature and surface wind fields associated with the Southern Oscillation/El Niño. *Mon. Wea. Rev.,* **110,** 354–384.

Slutz, R. J., S. J. Lubker, J. D. Hiscox, S. D. Woodruff, R. L. Jenne, D. H. Joseph, P. M. Steurer, and J. D. Elms, 1985: *Comprehensive Ocean–Atmosphere Data Set. Release 1.* NOAA Environmental Research Laboratory, Boulder, Colorado, 268 pp.

Vautard, R., and M. Ghil, 1989: Singular spectrum analysis in nonlinear dynamics, with applications to paleoclimatic time series. *Physica D,* **35,** 395–424.

von Storch, H., T. Bruns, I. Fischer-Bruns, and K. Hasselmann, 1988: Principal oscillation pattern analysis of the 30–60 day oscillation in a GCM equatorial troposphere. *J. Geophys. Res.,* **93,** 11 021–11 036.

——, U. Weese, and J.-S. Xu, 1990: Simultaneous application of space–time variability: Principal oscillation patterns and principal interaction patterns with applications to the Southern Oscillation. *Z. Meteor.,* **40,** 99–103.

Weare, B., and J. Nasstrom, 1982: Examples of extended empirical orthogonal function analyses. *Mon. Wea. Rev.,* **110,** 481–485.

Wilks, S., 1962: *Mathematical Statistics.* John Wiley & Sons, 644 pp.

Xu, J.-S., and H. von Storch, 1990: Predicting the state of the Southern Oscillation using principal oscillation pattern analysis. *J. Climate,* **3,** 1316–1329.